

Technical Paper

Classification and identification of surface defects in friction stir welding: An image processing approach



Ravi Ranjan^a, Aaquib Reza Khan^b, Chirag Parikh^c, Rahul Jain^d, Raju Prasad Mahto^d, Srikanta Pal^e, Surjya K. Pal^{d,*}, Debasish Chakravarty^f

^a Department of Electronics and Communication Engineering, Birla Institute of Technology, Mesra 835215, Ranchi, India

^b Department of Electrical and Electronics Engineering, Birla Institute of Technology, Mesra 835215, Ranchi, India

^c Department of Chemical Engineering, Birla Institute of Technology, Mesra 835215, Ranchi, India

^d Department of Mechanical Engineering, Indian Institute of Technology, Kharagpur 721302, India

^e Department of Electrical Engineering, Shiv Nadar University, Gautam Buddha Nagar 201314, India

^f Department of Mining Engineering, Indian Institute of Technology, Kharagpur 721302, India

ARTICLE INFO

Article history:

Received 27 January 2016

Received in revised form 7 March 2016

Accepted 9 March 2016

Available online 8 April 2016

Keywords:

Friction stir welding

Weld defects

Digital image processing

ABSTRACT

Friction stir welding (FSW) is a new entrant in welding technology and getting a defect-free weld is the final objective. But different defects are generated due to various reasons and needs to be analyzed to eliminate them. The aim of the research work is to identify and classify different kinds of surface defects generally encountered during the FSW process using digital image processing techniques. The defects on the surface of the weld are identified using image pyramid and image reconstruction algorithms. Further, using these algorithms the defects can be classified into voids, grooves, cracks, key-hole and flash with the help of unique features of each kind of defect. Vertical intensity plot and the area plot of the defect blobs are represented for the proper localization and analysis of severity of defects.

© 2016 The Society of Manufacturing Engineers. Published by Elsevier Ltd. All rights reserved.

1. Introduction

The friction stir welding process (FSW) is comparatively a new entrant in the welding technology. This solid state joining process was invented by The Welding Institute (TWI) in 1991 [1]. The process is simple, eco-friendly and energy efficient, and has wide applications in various industrial areas such as automobile, aircraft and aerospace industries, as it can weld low density material like aluminum and magnesium efficiently [2,4,5]. It is observed that the FSW joints have high strength; almost close to the base metal and also helps in weight savings considerably than the other joining processes as no filler material is added during welding. It is reported that during FSW there is no presence of a state of liquid weld pool and thus temperature rise in FSW is less and is nearly 0.7–0.9 times the melting temperature of the metal [3–5].

Weld quality is affected because of various kinds of defects occurring during the FSW process. A good amount of efforts are being made in this regard to identify the defects in welding.

Several researchers have worked on the analysis of surface defects in the FSW process. Defects like cavity, surface grooves and

flash could occur due to inappropriate set of process parameters which results in excessive or insufficient heat input or abnormal stir [3]. Kim et al. [6] reported that, volumetric defects develop in FSW at colder process parameters like low rotational and high transverse speed. Sizes of these defects depend on the magnitude of forging forces in force control mode. Insufficient forging force can result in extended grooves on the surface which may be discontinuous, periodic or continuous. They pointed out that at low rotational speed, wormhole (void) develops in advancing side because at low rotational speed heating is not sufficient, and hence less material stirring occurs nearby nugget zone. Chen et al. [7] studied effect of tool tilt angle on welding defect on AA5456 aluminum alloys. They observed long groove defect along advancing side on top surface and void in nugget zone. However, at higher tilt angle, 2–3°, they observed good results but on contrary at 4–5°, channel defects are observed below the nugget zone along the advancing side and more flash observed in retreating side. Defect analysis in FSW could be done by several non-destructive methods like immersion ultrasonic and phase array ultrasonic techniques [8], X-ray radiography [9], thermography [10], eddy current testing [11], synchrotron radiation [12], etc. In phase array ultrasonic technique, defects like cracks and voids could easily be detected by the excitation of piezo-composite element which can generate focused beam where beam's parameters like angle and focal distance can also be

* Corresponding author. Tel.: +91 3222 282996; fax: +91 3222 255303.

E-mail addresses: skpal@mech.iitkgp.ernet.in, surjya.pal@gmail.com (S.K. Pal).

modified [8]. Saravanan et al. [9] studied the effect of welding parameters like rotational speed, penetration depth and travel speed by using X-ray radiography technique which was able to detect micro-pores, voids and a tunnel defect in friction stir weld of aluminum-zinc coated steel lap joints. Mezyk and Kowieski [10] used thermographs of the FSW weld surface including burrs, discontinuities and uneven edges. Surface and sub-surface defects present in the weld were identified with the help of temperature plots extracted along the cross-section of the weld from thermally recorded sequence of images.

In welding processes, several researches have been made to detect the defects using the image processing techniques. In gas arc welding, it becomes difficult to capture clear images because of the bright welding arc, which makes the welding environment harsh. In order to detect the shape and size of the droplet more accurately, several image processing techniques like bilinear interpolation, double threshold, moving kernel filter algorithm, etc. have been used [13–16]. In comparison to the gas arc welding, images acquired in the FSW process does not have the above issues of lighting conditions and the images captured are more clear and do have high resolutions. Therefore, different image processing techniques like image pyramid, image reconstruction have been used in this research work.

Texture analysis techniques used for analysis of machined surfaces help in determining the surface roughness and weld quality analysis [17]. Sinha et al. [18] used image processing techniques like contour plots and gray-level intensity plots along the length of the weld for comparing the changes in weld surface texture patterns in cases of tool pin failure and pin depth at the time of online monitoring of FSW. Researchers have also exploited the advantages of using image processing techniques over other invasive or non-invasive techniques (like linear profile plot and contour plots) to distinguish between a good and a defective weld [19]. Usage of digital image correlation technique has been reported for the analysis of weld surface quality by extracting first and second order statistical image parameters which showed clear variations in their intensities with respect to good and defective weld regions [20]. Bhat et al. [21] have applied discrete wavelet transform on weld images to identify to defective and good weld. They have achieved accuracy of 99% and 97% with Gaussian and polynomial kernel respectively. Cox et al. [22] have studied the effect of tool rotation on spot weld quality. They found a linear relation between tensile shear strength and number of tool rotation. Gibson et al. [23] discussed the various aspects of the FSW process including input variables, joint configurations, tool design, etc. They have also discussed about the various variant of the process like stationary shoulder, self-reacting, friction stir processing along with application of the process and future research scope. Kim et al. [24] developed an algorithm to predict weld quality using image processing during high frequency electric resistance welding. They have used a vision sensor to capture the image at the proximity of weld spot. Zhang et al. [25] have examined parameters from weld pool surface to determine the backside bead width measurement to identify the penetration during gas tungsten arc welding. They have used machine vision system to measure specular weld pool surface in real time.

Among the available literature on the analysis of the surface defects in FSW process, there is hardly any report on classification and exact localization on the type of surface defect. Until now, the image processing techniques have only been applied to analyze the weld texture quality. This research work mainly aims in identifying and classifying the type of surface defects into voids, grooves, rough texture or crack, flash and key-hole that usually occur during the welding process using image processing techniques. The image processing techniques applied in this research work, results in yielding the exact location of the surface defects. The output



Fig. 1. NC controlled friction welding machine.

produced by the proposed algorithm gives a vertical intensity plot of each kind of defect and an area plot of overall defects. Though the results obtained by the methodology proposed in this research work are carried out by taking offline images of the weld surface, it could be used in future online monitoring process, giving a feedback for controlling the welding parameters during the FSW process.

2. Experimental procedure

Experiments have been carried on a 2 Ton linear NC controlled FSW machine manufactured by ETA Bangalore, India Ltd., as shown in Fig. 1. The machine consists of strain gauge type load cell along Z and X axes to measure the reaction and welding force, respectively. Work piece material is AA1100, pure commercial alloy, whose composition is mentioned in Table 1. Work piece thickness is 2.5 mm and each work piece sample has a length and width of 100 and 40 mm, respectively. Tool is made up of tool steel H13 and has following dimensions: diameter of shoulder is 20 mm; diameter of pin is 5 mm; and the height of pin is 2.1 mm. Plunge depth in all experiments was kept at 0.1 mm with a spindle tilt angle of zero degrees. Flat tool shoulder is selected with cylindrical tool pin profile for the experiment. Rotational speeds for two different levels are chosen as 800 and 3000 rpm, while welding speeds at two different levels are 50 and 125 mm/min. Welding is performed in butt configuration and no pre or post treatment on weld sample is performed. Another welding has been performed to obtain the lap joint between AA6061-T6 sheet and AISI304 sheet each of thickness 1 mm. For this the FSW tool has a cylindrical pin whose diameter and height is 5 and 1 mm, respectively, whereas diameter of the shoulder is 18 mm. The shoulder part of FSW tool is made from H13 steel whereas the pin part is made up from tungsten carbide. All experiments for lap joint are carried out at a tilt angle of zero degree plunge depth of 0.2 mm. The aluminum sheet was placed over the steel sheet in each experiment with an overlap length of 30 mm. The weld sample shown in Fig. 11(a) was obtained at a rotational speed of 1800 rpm and a welding speed of 63 mm/min whereas the weld sample shown in Fig. 12(a) was obtained at a rotational speed of 1400 rpm and a welding speed of 31.5 mm/min. Detailed discussion on Fig. 11 and Fig. 12 are mentioned in the Section 4. The composition of both the materials used is mentioned in Tables 2 and 3. Images of the welded sample is taken with a digital camera in RGB format and cropped to the size of 2231 × 500. The entire image processing algorithm was developed in MATLAB 2012a.

Table 1

Chemical Composition of AA1100 Aluminum alloy (obtained from XRF test conducted in XRF machine S8 Tiger manufacture by Bruker).

Element	Al	Si	Fe	Mn	Cu	Ti	Mg	Zn	Ga	Na	P	Pb
Wt%	98.4	0.7066	0.842	0.013	0.00505	0.0048	0.00465	0.0031	0.0118	0.0024	0.0047	0.00189

Table 2

Chemical composition of aluminum alloy AA6061-T6.

Element	Al	Si	P	Mg	Ti	Cr	Mn	Fe	Cu	Zn
Wt%	98.36	0.72	0.01	0.03	0.01	0.18	0.05	0.35	0.28	0.01

Table 3

Chemical composition of steel AISI304.

Element	Fe	Si	P	S	V	Cr	Mn	Al	Co	Ni	Cu	Zn	C
Wt%	70.94	0.22	0.04	0.04	0.08	17.55	1.61	0.07	0.14	7.96	0.92	0.11	0.05

3. Theory and methodology

Watershed transform [26] locates ‘catchment basins’ in an image where the gray-level intensity is uniform and separates these regions where there is a change in gray-level intensity using ‘ridge lines’. This technique proved helpful to separate out voids and grooves like defect regions (structures) in a weld surface image, but it also separated out two different weld texture regions having slight gray-level intensity variation which was not desired. Other techniques like Adaptive threshold is very useful to segment out foreground objects from a non-uniformly illuminated background [27], but for a uniformly illuminated image of the weld surface it also segments out small texture variations appearing as cracks which was an undesirable outcome.

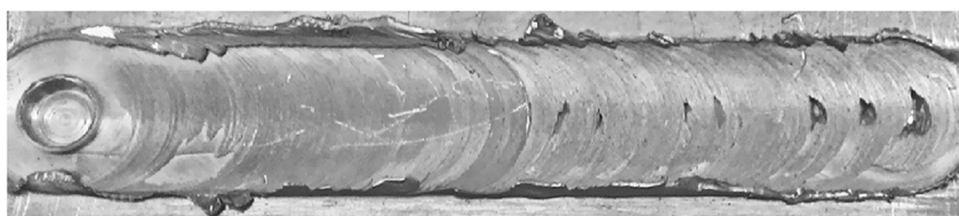
It was concluded that rough texture and cracks have entirely different characteristic features from voids, grooves and key-hole type defects; so it was better to use different image processing techniques for their identification. For the identification of voids, grooves and key-hole type defects, image reduction can be carried out using Fast Fourier Transform (FFT) and simple convolution of original image with its different scales. However, pyramid-based image reduction is efficient and faster to compute than FFT and convolution-based techniques [28]. Another way of achieving

image reduction is through scale space representation, but image pyramid does computationally efficient approximations as compared to scale-space representation. Data compression is possible to be achieved by pyramid encoding with quantization and entropy coding [28].

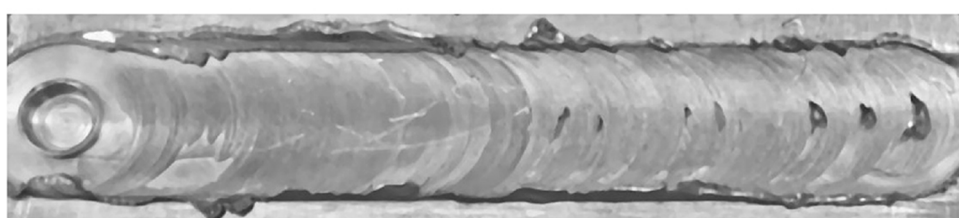
Segmentation of rough texture and cracks using Sobel edge detection method resulted in a lot of noise even due to minute variations in the texture of the weld surface. Contrast Limited Adaptive Histogram Equalization (CLAHE) technique increases the contrast of an image [29], thus emphasizing more upon the cracks and rough textures. But again the insignificant variations in texture become evident which is undesirable for better segregation of rough texture and cracks. Thus, image reconstruction method has been used to elude this issue. Image reconstruction rebuilds an image from its eroded variant such that all the insignificant variations in texture are removed [30].

3.1. Image pyramid-based processing

This part of image processing mainly deals with detection of defects like surface grooves, pin-hole and voids on the weld surface. The color image of the work piece was taken and was converted



(a). Original image of the welded sample



(b). Smoothened image of the welded sample

Fig. 2. (a) Original image of the welded sample. (b) Smoothened image of the welded sample.



Fig. 3. Defects (surface grooves, pin hole and voids) on the weld surface.

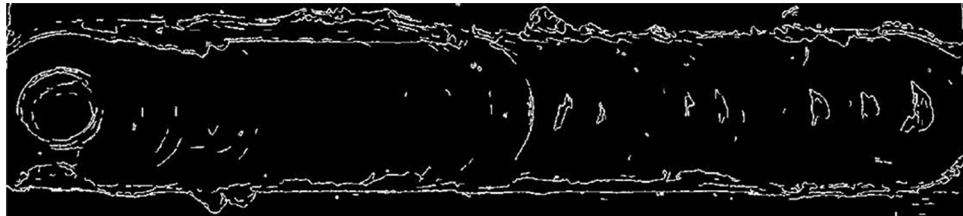


Fig. 4. Cracks and edges of grooves, voids detected on weld surface.

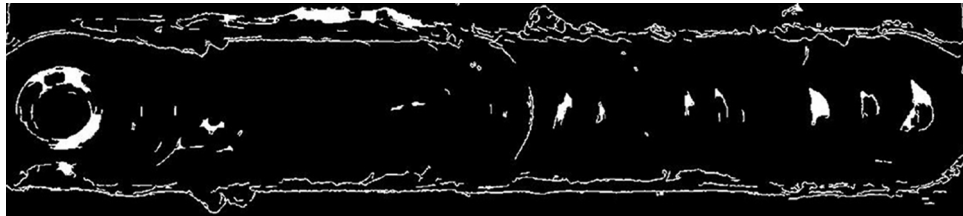


Fig. 5. Fused image having all types of surface defects.

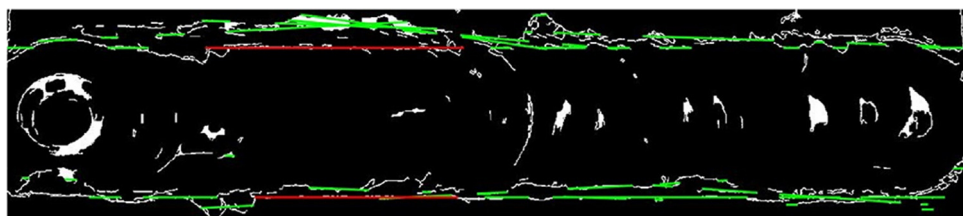
into grayscale image by having a weighted sum of the *R*, *G*, and *B* components [31]:

$$\text{Grayscale intensity} = 0.2989R + 0.5870G + 0.1140B \quad (1)$$

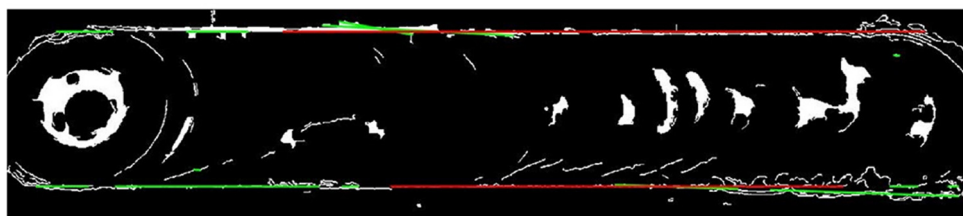
For better identification of defects, filtering operation of the grayscale image was carried out using two 2-dimensional median filters of order 5 and 10. A median filter reduces the salt and pepper noise from an image while preserving the edges and sharpness of the image [32]. This operation was carried out to have a smooth background texture and have clear visualization of defects in

foreground. The grayscale image of the weld is shown in Fig. 2(a) and that of corresponding median filtered image is shown in Fig. 2(b). Further processing of weld image has been done using image pyramid.

Image pyramid comprises of a set of low-pass or band-pass versions of an image, each depicting the pattern information of various scale [28]. This method is appropriate for data compression, image analysis and image enhancement as both spatial and frequency information of the image is retained. Moreover, image pyramid also reduces computation complexity of further image processing



(a). Straight lines (red) representing the edges of the weld



(b). Straight lines (red) representing the edges of the another weld(For interpretation of the references to color in this figure legend, the reader is referred to the web version of this article.).

Fig. 6. (a) Straight lines (red) representing the edges of the weld. (b) Straight lines (red) representing the edges of the another weld(For interpretation of the references to color in this figure legend, the reader is referred to the web version of this article.).

operations, as the both sample density and resolution are reduced, which is critical to online monitoring applications. Different levels of pyramid can be acquired as follows. For $0 < l < N$:

$$G_l(i, j) = \sum_m \sum_n w(m, n) G_{l-1}(2i + m, 2j + n) \quad (2)$$

where, G_0 is the bottom level of the pyramid, i.e., the original image, $w(m, n)$ is the weighting function or the generating kernel and N is the number of levels in the pyramid.

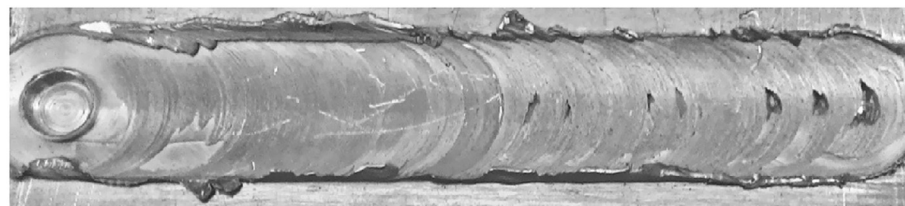
The kernel should be selected in such a way that it is smaller in size, symmetric and separable in order to reduce the computational time [33]. The kernel chosen is based on Eq. (3).

$$w = \left[\frac{1}{4} - \frac{a}{2}, \frac{1}{4}, a, \frac{1}{4}, \frac{1}{4} - \frac{a}{2} \right] \quad (3)$$

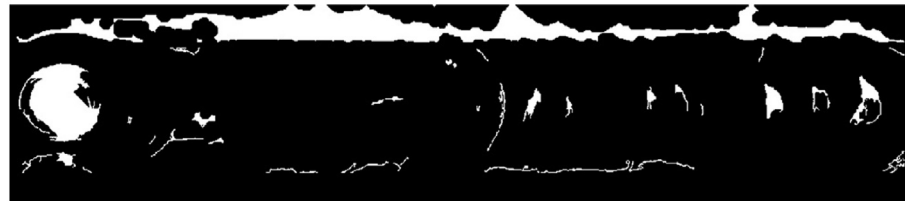
where, $a = 0.375$ so that the kernel is approximately same as Gaussian shape providing low pass filtering. The low pass filtering allows further sub-sampling of image without losing information, thus the signal strength remains intact and signal to noise ratio remains high. Whereas on resizing the image the signal to noise

ratio gets reduced, thus reduction using image pyramid is better where the quality of the image is preserved.

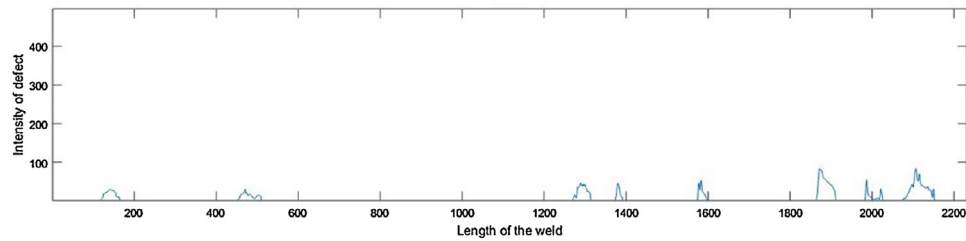
So, pyramid-based expansion and reduction of image has been carried out in order to enhance or diminish the resolution of image [33]. Initially pyramid-based reduction of the image has been done so that small texture variations (due to onion rings) and cracks appearing in the image are removed and only prominent features left in the image are grooves, voids and pin-hole. Sobel edge detection have further been used which detects edges by using Sobel approximation on the derivative. The edges are returned at the points having the maximum gradient in the image [34]. This operation makes edges around all the defects occurring in the welded work piece. The output of this operation is a black and white image. Finally, some of the morphological operations (as listed below) have been applied to make a blob around the regions having defects as shown in Fig. 3. The structuring elements used for all the morphological operations are disk shaped and are of size 5 and 7, which was selected after optimizing the result after 30 samples.



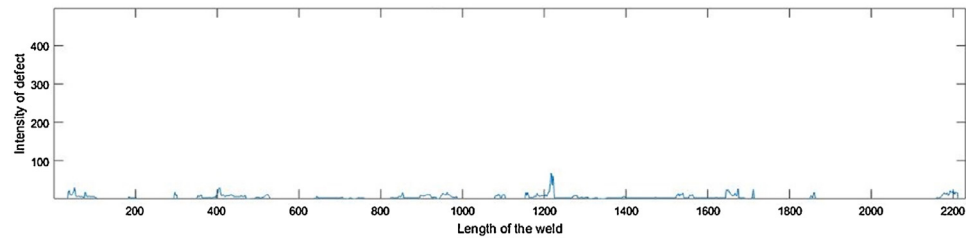
(a). Image of the original defect weld



(b). Output image with all the surface defects

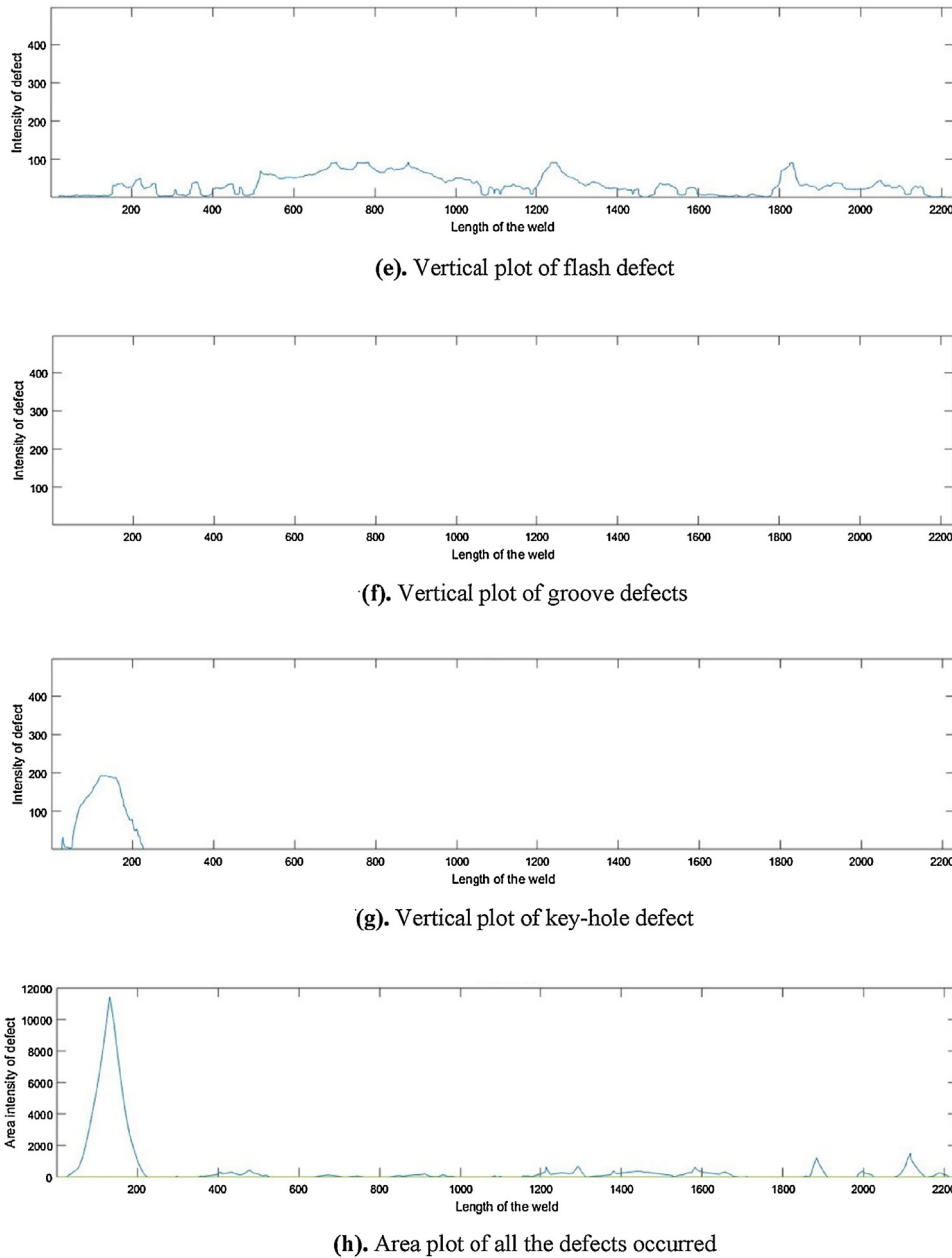


(c). Vertical plot of voids



(d). Vertical plot of rough texture and cracks

Fig. 7. (a) Image of the original defect weld. (b) Output image with all the surface defects. (c) Vertical plot of voids. (d) Vertical plot of rough texture and cracks. (e) Vertical plot of flash defect. (f) Vertical plot of groove defects. (g) Vertical plot of key-hole defect. (h) Area plot of all the defects occurred.

**Fig. 7. (Continued).**

Morphological operations:

- (1) Dilation: It is a transformation of the binary image in which the boundaries of the regions of the foreground pixel is gradually enlarged [35].
- (2) Erosion: It is a transformation of the binary image in which the boundaries of the regions of the foreground pixel is gradually reduced [35].
- (3) Morphological opening: It is the process in which erosion is followed by dilation, employing same structuring element. It helps in removing small objects preserving the shape and size of larger objects in an image [35].
- (4) Morphological closing: It is the process in which dilation is followed by erosion, employing same structuring element.

3.2. Image reconstruction-based processing

The ultimate aim of this processing was to detect cracks and edges which could not be possibly detected in the above discussed

process. Image reconstruction algorithms can be applied to both binary and grayscale images, while we have used it for the grayscale images of the weld sample.

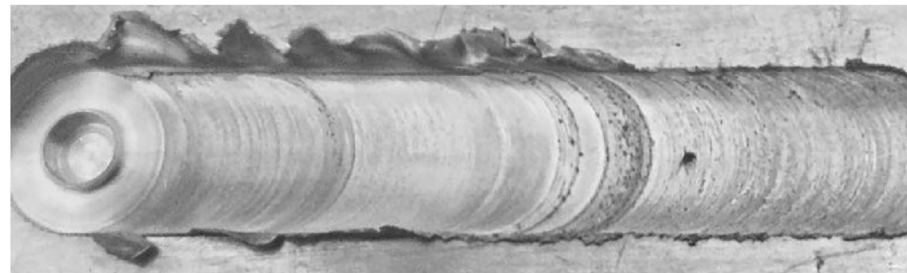
Grayscale image reconstruction is basically defined as the reconstruction of the mask image by successive geodesic dilations of a marker image until its contour fits under the mask image and such that the grayscale values of every pixel of the marker image is less than or equal to that of the mask image. The reconstruction algorithm requires the type of grid to define its way of traversal, like 4-connectivity, 8-connectivity, etc. It also uses a flat structuring element of size n ($n \geq 0$).

This research work uses fast hybrid grayscale reconstruction algorithm which was developed by the combination of the sequential reconstruction with the regional maxima-based reconstruction algorithm using breadth first scanning enabled by a queue of pixels [30]. The algorithm has wide applications and the authors have used it to remove insignificant or false texture variations occurring during Sobel edge detection and also retaining the actual

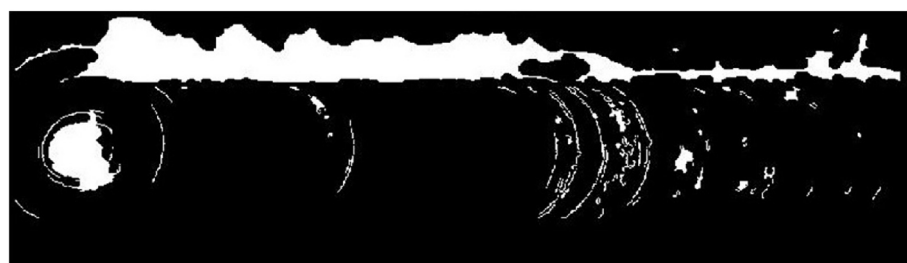
edges, cracks and rough texture variations on the weld surface. On the contrary, while removing these false or noisy features, morphological opening fails to retain the original features. Thus this algorithm is better than morphological opening and is also

computationally efficient which is good enough for online monitoring process.

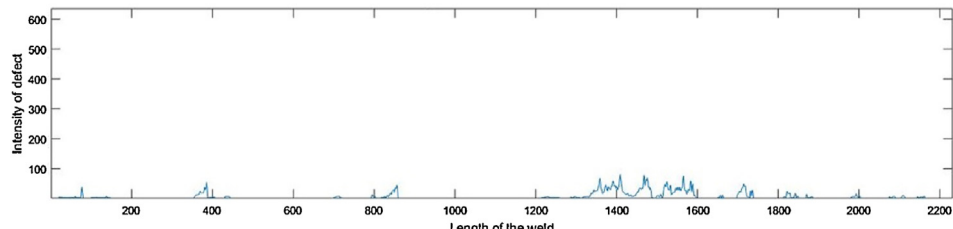
Here, the grayscale image of the original weld sample was used as the mask image while its eroded image was used as the marker



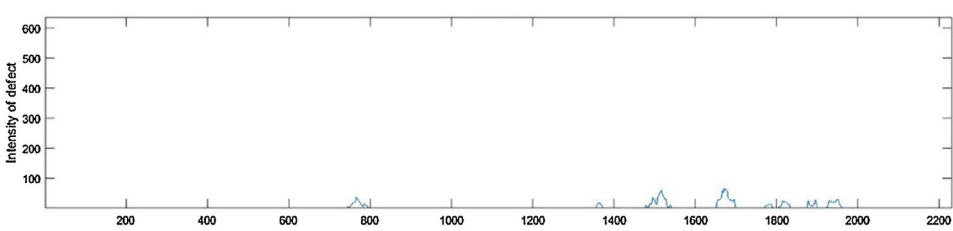
(a). Image of the original defect weld



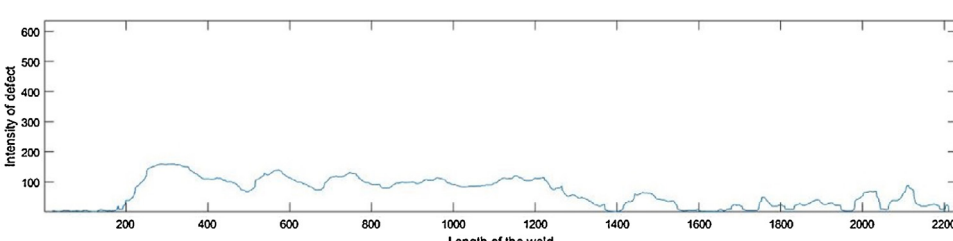
(b). Output image with all the surface defects



(c). Vertical plot of rough texture and cracks



(d). Vertical plot of voids



(e). Vertical plot of flash defects

Fig. 8. (a) Image of the original defect weld. (b) Output image with all the surface defects. (c) Vertical plot of rough texture and cracks. (d) Vertical plot of voids. (e) Vertical plot of flash defects. (f) Vertical plot of groove defect. (g) Vertical plot of key-hole defect. (h) Area plot of all the defects occurred.

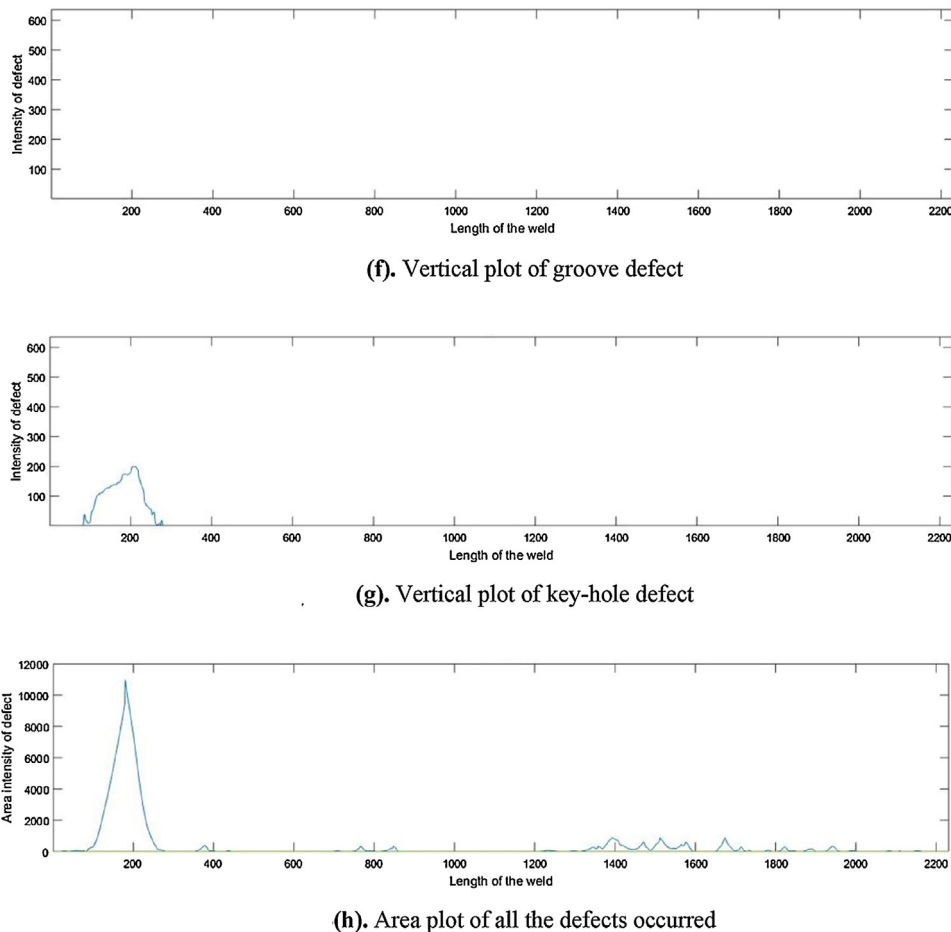


Fig. 8. (Continued).

image for image reconstruction with 4-connectivity. Erosion of the grayscale image has been done with the disk shaped structuring element of size 20 such that to ensure that the insignificant features are removed while the actual features remain marked. For further smoothening and noise reduction, 2-dimensional median filter of order 5×5 was applied on the reconstructed image. The filtered image was then used for edge detection. All the edges (like cracks, boundary of voids and surface grooves, onion rings, etc.) in the image was detected by applying Sobel approximation on to the derivative, which gives edges at the point of maximum gradient of the image. The results also include edges of the flash at the retreating side of the weld which is discussed in subsequent sections of this research work. Furthermore, remaining noise was eliminated by using the 'bwareaopen' function of MATLAB [27] and finally, the image was further dilated using the diamond shaped structuring element of size 1 to get the desired output. Thus, this process was helpful in detecting cracks, rough texture, edges of flash and detecting boundaries of the retreating side as well as the advancing side on the weld surface as shown in Fig. 4.

The shape and size of the structuring elements used in the above two methods for various morphological operations have been optimized from 30 weld samples and finally kept fixed in all the weld samples proving the robustness of the algorithm. These parameters have been optimized such that maximum accuracy is achieved in the defect identification.

3.3. Image fusion

The former image processing algorithm was used to effectively detect surface grooves, voids, cavities and the key-hole on the

surface of the weld, while the latter was used to effectively detect cracks and flash formations on the retreating side of the weld surface. The output binary images of the above two algorithms (containing different types of surface defects) was merged (or fused) into a single binary image which contained all kinds of surface defects in the form of white blobs as shown in Fig. 5.

3.4. Hough transform

As the flash defects are generally spread all along the length of the weld on the retreating side, it was better to analyze them separately. Moreover, for making the contemplated algorithm free from human intervention it was also needed to detect the advancing side of the weld so that the image processing required for identification of other defects could be carried out between retreating and advancing side of the weld region only. By using Hough Transform, a ROI (Region of Interest) was made around the entire retreating side of the weld for analysis of flash defects and another ROI was made between retreating and advancing side of the weld for the identification of other types of defects.

This feature extraction technique is used to detect straight lines in an image [31]. It uses parametric equation of the straight lines, as given in Eq. (4).

$$\rho = x \cos \theta + y \sin \theta \quad (4)$$

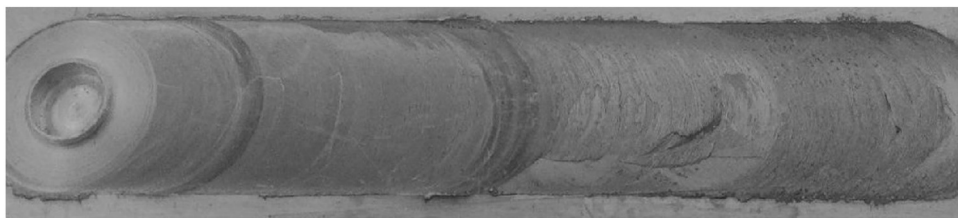
The distance from the origin to the line along a vector perpendicular to the line is designated as ρ , and the angle between the X-axis and this vector is represented by θ . The Hough transform of a binary image gives a set of straight lines in pairs of (ρ, θ) in the Hough transform matrix with each pair having a particular peak

value representing the number of points through which the line crosses [31].

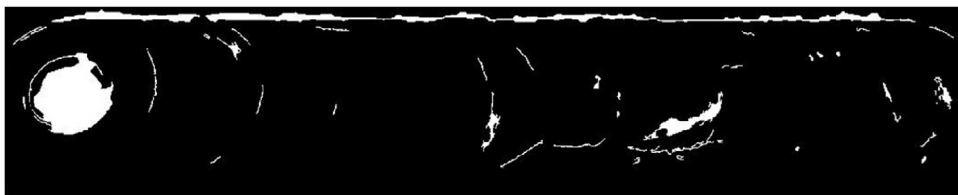
To extract straight lines from a binary image using Hough transform, the Hough transform matrix, θ matrix and the ρ matrix are initially computed. In order to separate out potential straight lines from the image, peak values were located in the Hough transform matrix above a particular threshold. The threshold for peak values, i.e., the number of points which lies on a straight line was decided to be 0.3 times the number of points lying on the longest possible straight line in the image, i.e., $0.3 \times$ maximum of Hough transform matrix. Also, the minimum length of the line should be greater than 10 pixels.

Using these peak values and θ and ρ matrices, all the potential straight lines were obtained from the binary image. Since, the edges of the weld have sharp contrast and are nearly horizontal,

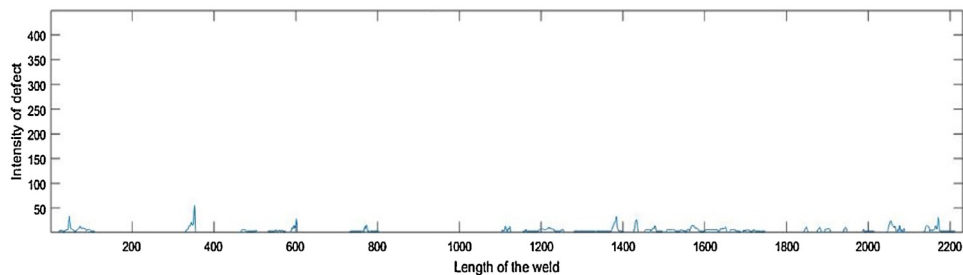
the longest straight lines having a slope value ranging from -5° to 5° would represent the edges of the weld. Complying with the above conditions, maximum peak value was searched separately in the lower and upper half of the image to represent the lower and upper edge of the weld. After implementing this method, all the probable straight lines are shown with green lines and the edges of the weld are shown with red lines in Fig. 6(a). As the flash defect lies on the retreating side just above the edge of the weld, an ROI was made above this longest line obtained using Hough transform. This ROI was used to generate a separate image (i.e., image above the edge) for the analysis of flash defects. In order to show the repeatability of this method, image of another weld sample is shown in Fig. 6(b) with green lines showing probable straight lines and red lines representing the edges of the weld.



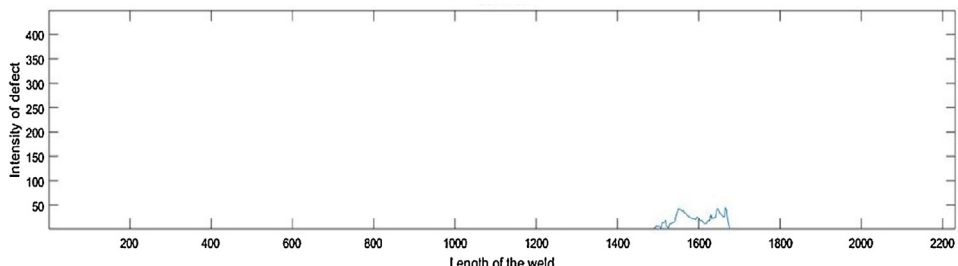
(a). Image of the original defect weld



(b). Output image with all the surface defects



(c). Vertical plot of rough texture and cracks



(d). Vertical plot of groove defect

Fig. 9. (a) Image of the original defect weld. (b) Output image with all the surface defects. (c) Vertical plot of rough texture and cracks. (d) Vertical plot of groove defect. (e) Vertical plot of voids. (f) Vertical plot of flash defects. (g) Vertical plot of key-hole defect. (h) Area plot of all the defects occurred.

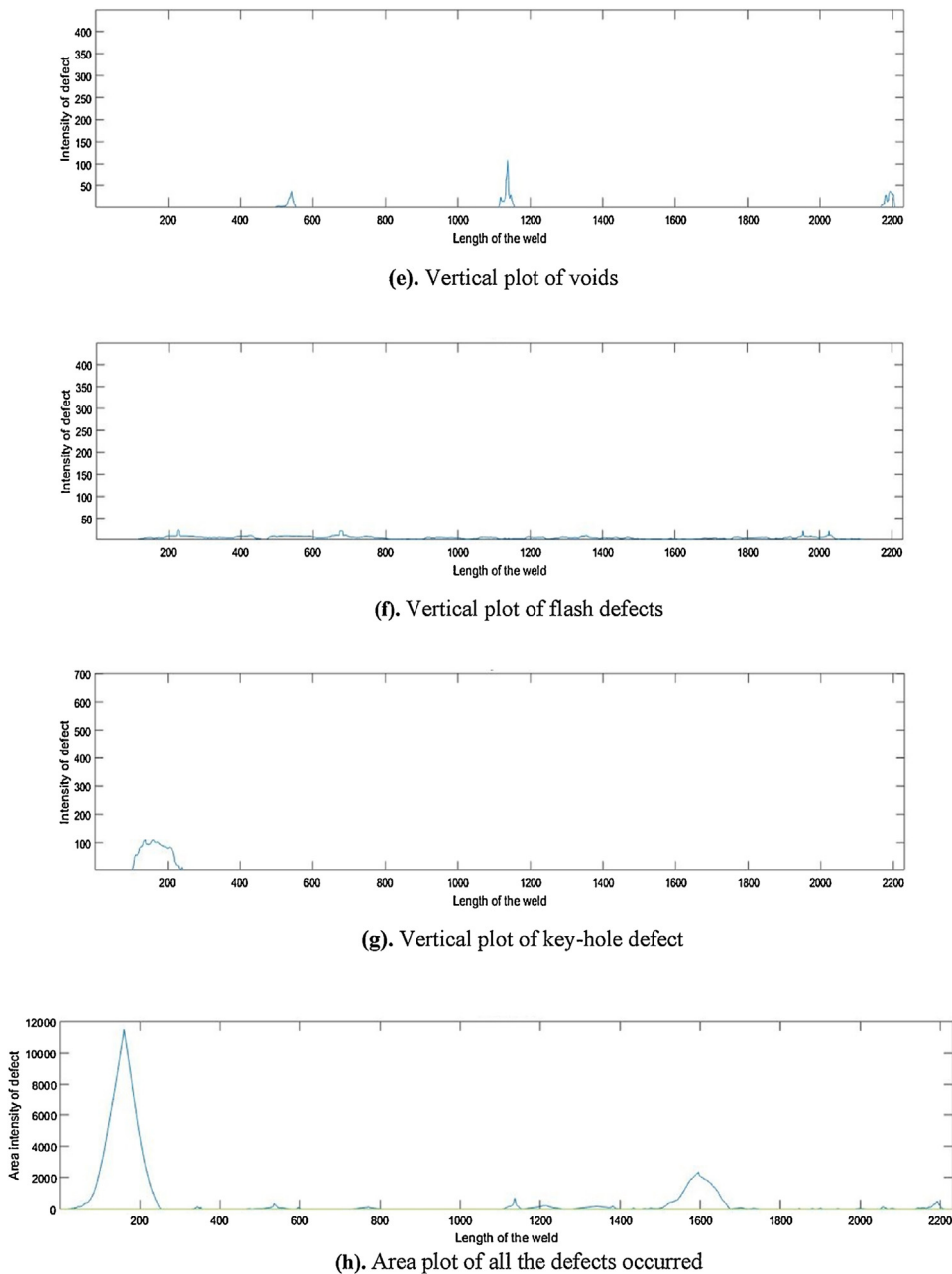


Fig. 9. (Continued).

3.5. Classification of surface defects

After using various image processing techniques for the segmentation of (all kinds of) surface defects from the weld surface image, they could be further classified into voids, grooves, cracks, flash and key-hole defects. The two images extracted from the original binary image using Hough transform viz. the image part above the edge on the retreating side of the weld and the image part below this edge and above the advancing side were used separately to analyze different kinds of defects. The image above the retreating side consists of only flash defects which separates it from all other defects which are present in the image below this edge. Furthermore, image below this edge was used for classifying all other defects like voids, grooves, cracks and key-holes. Features like length of major axis, orientation of major axis, ratio of total area to the length of major axis, and the ratio of length of major axis to that of minor axis of the ellipse formed around the defect blobs oriented

at any angle were used to classify different kinds of defects. Length of major axis of the blob signifies the length of the defect along the oriented angle. The ratio of total area to the length of major axis of the blob signifies the average width of the blob along the orientation of minor axis (of the ellipse) formed around the defect blobs. The ratio of length of the major axis to that of minor axis signifies the circular nature of the blob. The following five types of features were identified using the proposed approach.

- (1) Flash: After applying certain morphological operations of dilation, filling and erosion on the image above line, flash formed during the weld was analyzed. A vertical histogram plot was generated which represented the variation in intensity and the localization (or location) of flash defect along the length of the weld.
- (2) Cracks and rough texture: Cracks are generally narrower than voids and grooves. So, the average width feature was used

for the classification of cracks from all other defects. A lower threshold value of the average width (<5 pixels) of the defect blob was given to classify cracks from all other defects (like voids, grooves and key-hole) which always have an average width value greater than this threshold. This threshold yields maximum accuracy of crack detection.

- (3) Key-hole: The ellipse formed around this defect is likely to be circular. So, the ratio of length of major axis to that of minor axis will be nearly 1. Therefore, a threshold value (circularity ≤ 2) was given for this feature, which helped in determining a key-hole defect in the image below the edge of the weld. Also for a particular resolution of the image, the major axis length of the key-hole defect blob would always lie in the range of

65–350 pixels. Also, for carrying out faster identification of this defect, it was examined in a specific ROI near the end of the weld.

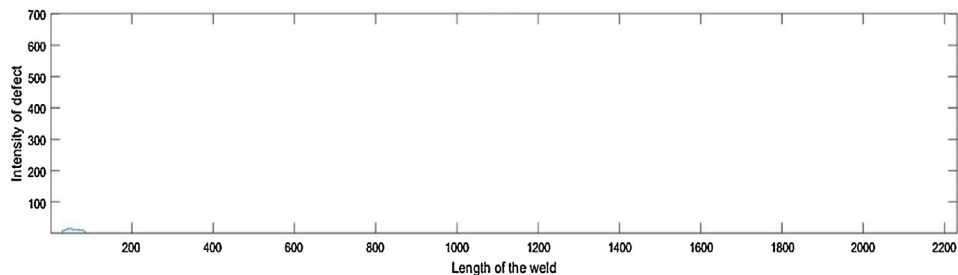
- (4) Grooves: Generally grooves are longer and horizontal; therefore, its classification was done using the length of major axis and its orientation (of the ellipse) formed around that blob. Hence, the defect blobs having quite a larger major axis length (≥ 35 pixels) as well as orientation in the range of -25° to 25° were classified as grooves.
- (5) Voids: Voids are the defects having variable size and could be oriented at any angle. It does not have any particular feature which could be used for its classification. Therefore, the remaining defect blobs were classified as voids.



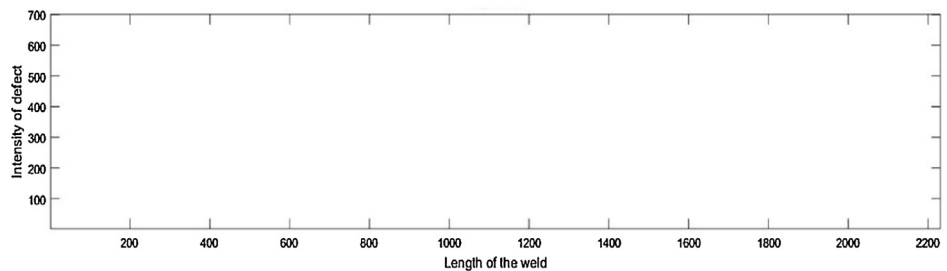
(a). Image of the original good weld



(b). Output image for the good weld

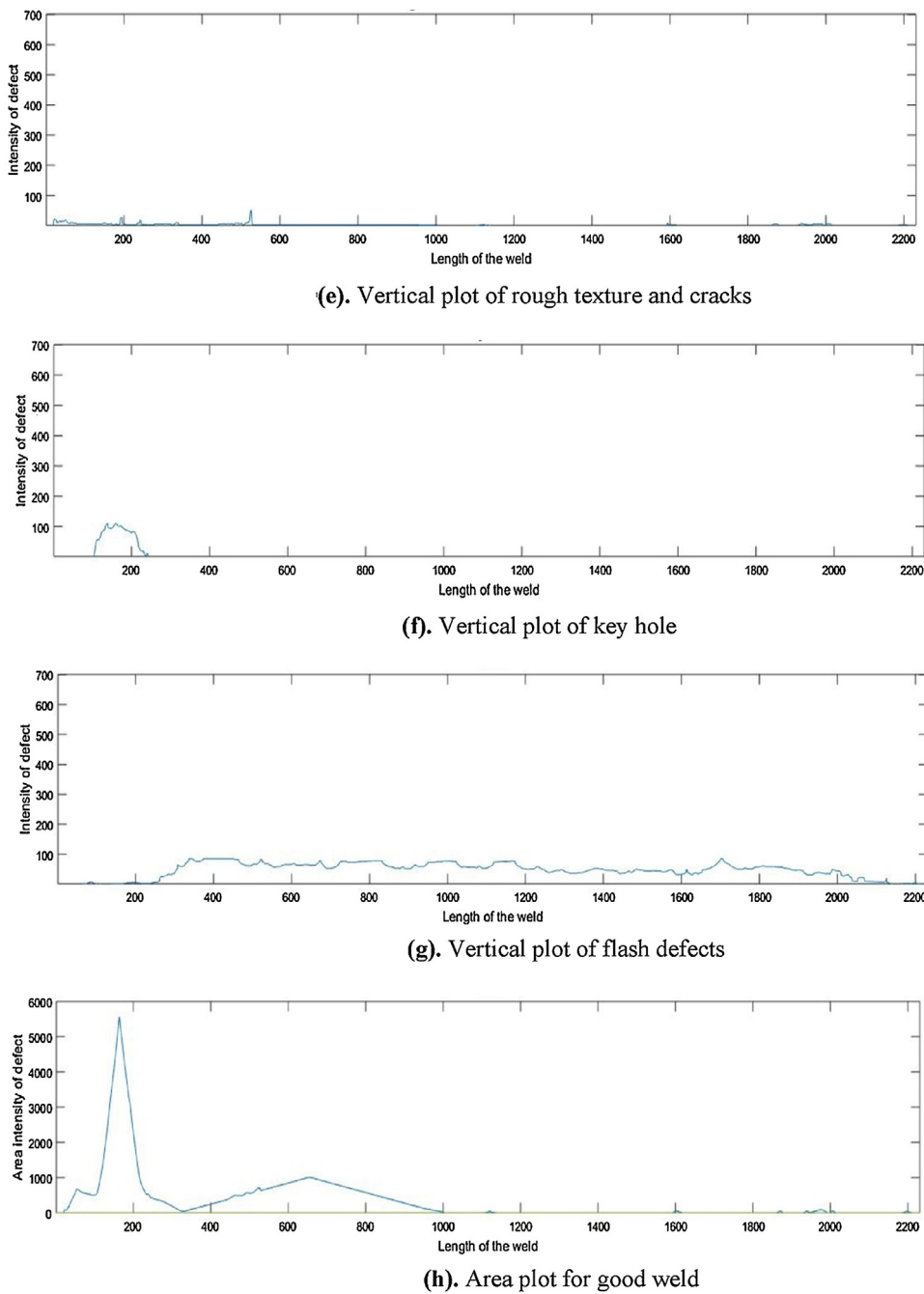


(c). Vertical plots of voids



(d). Vertical plot of groove defect

Fig. 10. (a) Image of the original good weld. (b) Output image for the good weld. (c) Vertical plots of voids. (d) Vertical plot of groove defect. (e) Vertical plot of rough texture and cracks. (f) Vertical plot of key-hole. (g) Vertical plot of flash defects. (h) Area plot for good weld.

**Fig. 10.** (Continued).

All the threshold values used are fixed for all samples and were decided by testing our algorithm with 30 weld images such that maximum accuracy of defect classification was achieved. The methodology used above requires the image of nearly same resolution for proper classification of surface defects. This was easily achieved by installing the camera at a specific location such that it always captures a fixed area of the weld portion. A fixed lighting condition was also ensured for maintaining a uniform luminous intensity all over the weld surface.

3.6. Area plot of all the defects

The image below the edge of the weld containing many defect blobs was used for further analysis of all other kinds of defects. These white blobs were labeled and the centroid, area,

bounding-box, major and minor axes lengths and orientation of the major axis line of ellipse formed around each blob was evaluated [31]. A histogram plot of the area of each defect vs. its corresponding Y-coordinate across the length of the image (across the length of the weld) was done. This area plot of each defect blob was done across the whole length of the blob (under the bounding-box) with the net area gradually increasing from its sides such that the total area of each blob would appear to be accumulated (or would be plotted) at the (Y-coordinate) centroid (centre of mass) of the blob as a maxima.

Finally, these area plots of each blob (defected regions) was superimposed to get (determine/evaluate) the final histogram plot of the whole weld surface image representing all kinds of defected regions in the form of different peak values of areas at their respective Y-coordinates of their centroids.

This area plot of the output binary image below the edge of the weld was done to get the amount, extent and the exact position of all the defected regions representing the percentage of good or bad weld according to a rough or smooth texture of a particular section of the weld surface.

4. Results and discussion

The methods for spotting out surface defects and their classification mentioned in the previous section is applied on a defective weld image using MATLAB software tool, and the output is shown in Fig. 7(a-h).

The image in Fig. 7(a) shows the original weld surface and Fig. 7(b) shows a black and white image in which all the identified surface defects have been represented as white blobs. The plots from Fig. 7(c) to Fig. 7(g) depict the magnitude and exact position of various classified defects with Y-axis representing the intensity in terms of number of white pixels in the output image, appearing

for a particular class of surface defects and X-axis representing the location of defects in terms of horizontal pixel value of the original image. Finally, the plot in Fig. 7(h) depicts the intensity and location of all the surface defects occurred during welding. The area plot has an advantage that all the peaks in the plot represents a specific surface defects and even the defects lying one above another in a particular cross section are distinguished separately. The peaks in the vertical plot of voids as shown in Fig. 7(c) represent the exact location and the intensity of voids occurred during the weld which can be easily verified from the original image of the weld. The presence of rough texture and cracks is also depicted successfully in the plot shown in Fig. 7(d). The appearance of flash throughout the weld is easily noticeable in the plot of Fig. 7(e). It can be observed that no peaks are there in the vertical plot of groove, as shown in Fig. 7(f) as the weld surface did not have grooves. The presence of key-hole is also depicted successfully in the plot shown in Fig. 7(g).

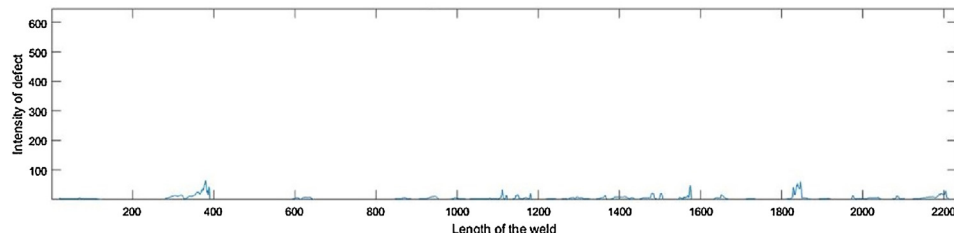
The output of surface defect identification and classification for another bad weld is shown from Fig. 8(a-h):



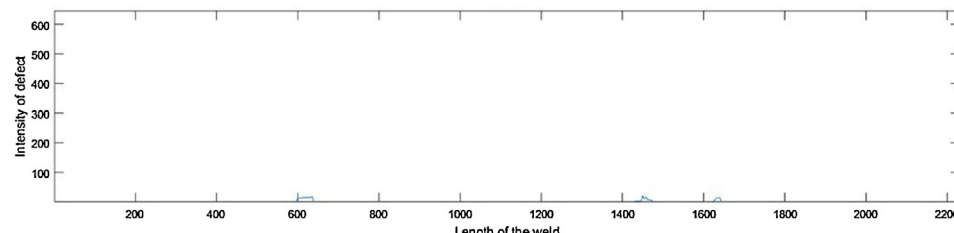
(a). Image of the original defect weld



(b). Output image with all the surface defects



(c). Vertical plot of rough texture and cracks



(d). Vertical plots of voids

Fig. 11. (a) Image of the original defect weld. (b) Output image with all the surface defects. (c) Vertical plot of rough texture and cracks. (d) Vertical plots of voids. (e) Vertical plot of groove defect. (f) Vertical plot of flash defects. (g) Vertical plot of key-hole. (h) Area plot of all the defects occurred.

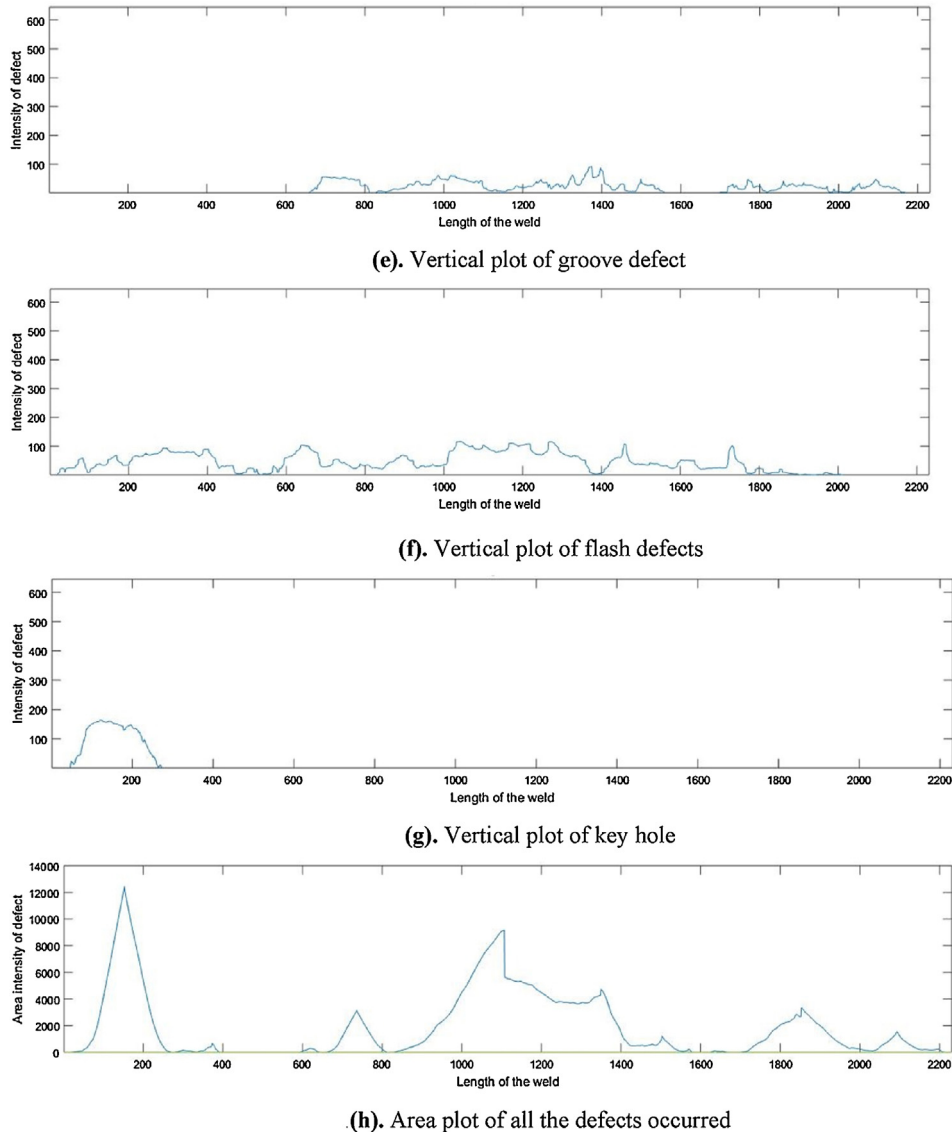


Fig. 11. (Continued).

In plots from Fig. 8(c-h), similar behavior can be observed with some more peaks in the vertical plot for rough texture and cracks as can be noticed in the original image of the weld. Again the vertical plot for grooves does not contain any peak as there were no groove defects in the original weld. High amount of flash, due to high heat input, can also be observed and is accurately depicted in the vertical plot of flash defect shown in Fig. 8(e).

The output of one more bad weld investigated in the present study with the proposed approach is shown from Fig. 9(a-h) to show the efficiency and accuracy of algorithm.

The rough texture and cracks occurred during the weld is perceptible in the plot of Fig. 9(c). The plot of Fig. 9(d) clearly shows the intensity and location of groove that has occurred around the middle of the weld. Two small voids observed at the end of weld is distinctly depicted by the plot of Fig. 9(e). A slight amount of flash, as observed in Fig. 9(a) is also depicted in the plot of Fig. 9(f). Lastly, the area plot delineating all the defects occurred during the weld is shown in plot of Fig. 9(h).

Finally, the algorithm is tested for a good weld and the output is shown from Fig. 10(a-h).

A small amount of salt and pepper noise can be observed in the output image shown in Fig. 10(b) due to irregular illumination

of the original weld surface. The vertical plot of voids, grooves, rough texture and cracks shown in Fig. 10(c-e) respectively clearly illustrate that no groove, void or rough texture and crack are found as expected from a good weld. Only flash defect is observed due to excessive heat input which is evident from the plot of Fig. 10(g).

Further, In order to prove that the proposed algorithm is material independent experiments were carried out to obtain the lap joint between AA6061-T6 (Aluminum) sheet and AISI304 (Steel) sheet each of thickness 1 mm. The images of weld were taken and processed for defect identification and classification and the results obtained are shown below:

It can be easily observed from Fig. 11(b) that all the defects were accurately discerned. Furthermore, plot of Fig. 11(e-g) distinctly shows the intensity and location of grooves, flash and key-hole respectively whereas plot of Fig. 11(c and d) shows that the weld sample does contain significant crack and void in it. Eventually the area plot characterizing all the defects along with their intensity in a single plot is shown in Fig. 11(h).

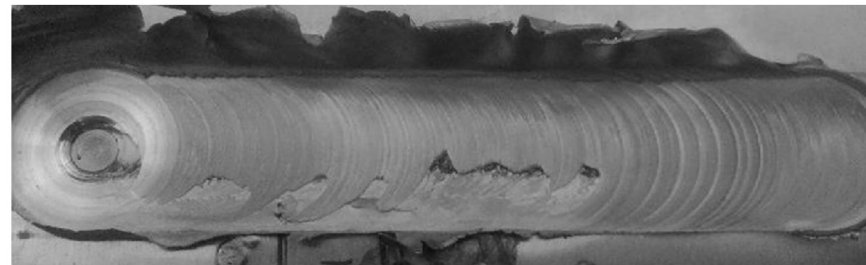
In order to show the robustness and generality of algorithm for material independency the result of another sample of lap joint

between aluminum alloy (AA6061-T6) and steel (AISI304) is shown below from Fig. 12(a–h). In this sample also all the defects were correctly recognized and located.

Again, it can easily be observed from Fig. 12(d, f and g) shows the intensity and location of grooves, flash and key-hole respectively whereas plot of Fig. 12(c and e) shows that the weld sample does contain significant crack and void in it. Also, the area plot characterizing all the defects along with their intensity is shown in Fig. 12(h).

In previous works, generally a sample image of the weld surface was taken and then cropped suitably for further processing and only the weld zone, excluding key-hole, flash, was analyzed. Therefore, a weld surface even with flash defects was regarded as an overall good weld. But actually, greater flash occurring on the retreating side of the weld weakens the strength of the welding zone resulting in a bad weld. The methodology discussed in this research work considers this flash defect by detecting retreating

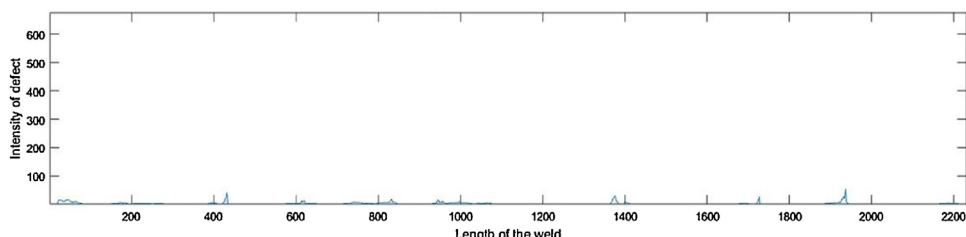
side edge of the weld. Also, considering future aspects of online monitoring, cropping the weld surface from the captured image is not feasible. So, by using Hough transform, edges of the weld (advancing and retreating sides) are detected as straight lines. Using the coordinates of these straight lines, weld surface is extracted from the captured image and hence, further processing could be done on it. Also, the methodology used is independent of the type of weld joint as well as the type of material used for welding. This research work has the potential of online monitoring as along with the identification and exact localization of the defects, it also focuses on the classification of defects which could be used in the online monitoring process of FSW. Also, the execution time of the MATLAB code is approximately 3.9 s per frame and hence, the welding parameters could be improved accordingly, as the traverse speed hardly goes beyond 200 mm/min depending on the type of surface defect and its severity for better quality weld results.



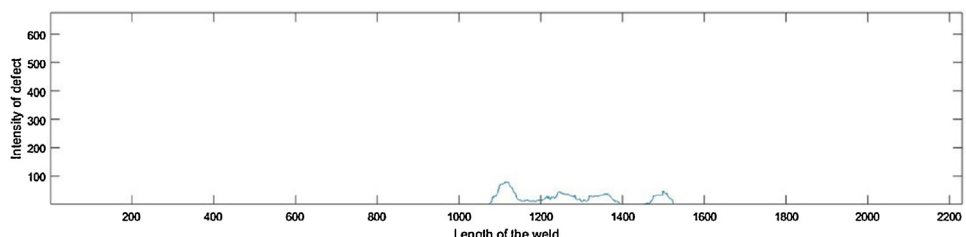
(a). Image of the original defect weld



(b). Output image with all the surface defects



(c). Vertical plot of rough texture and cracks



(d). Vertical plot of groove defect

Fig. 12. (a) Image of the original defect weld. (b) Output image with all the surface defects. (c) Vertical plot of rough texture and cracks. (d) Vertical plot of groove defect. (e) Vertical plots of voids. (f) Vertical plot of flash defects. (g) Vertical plots of key-hole. (h) Area plot of all the defects occurred.

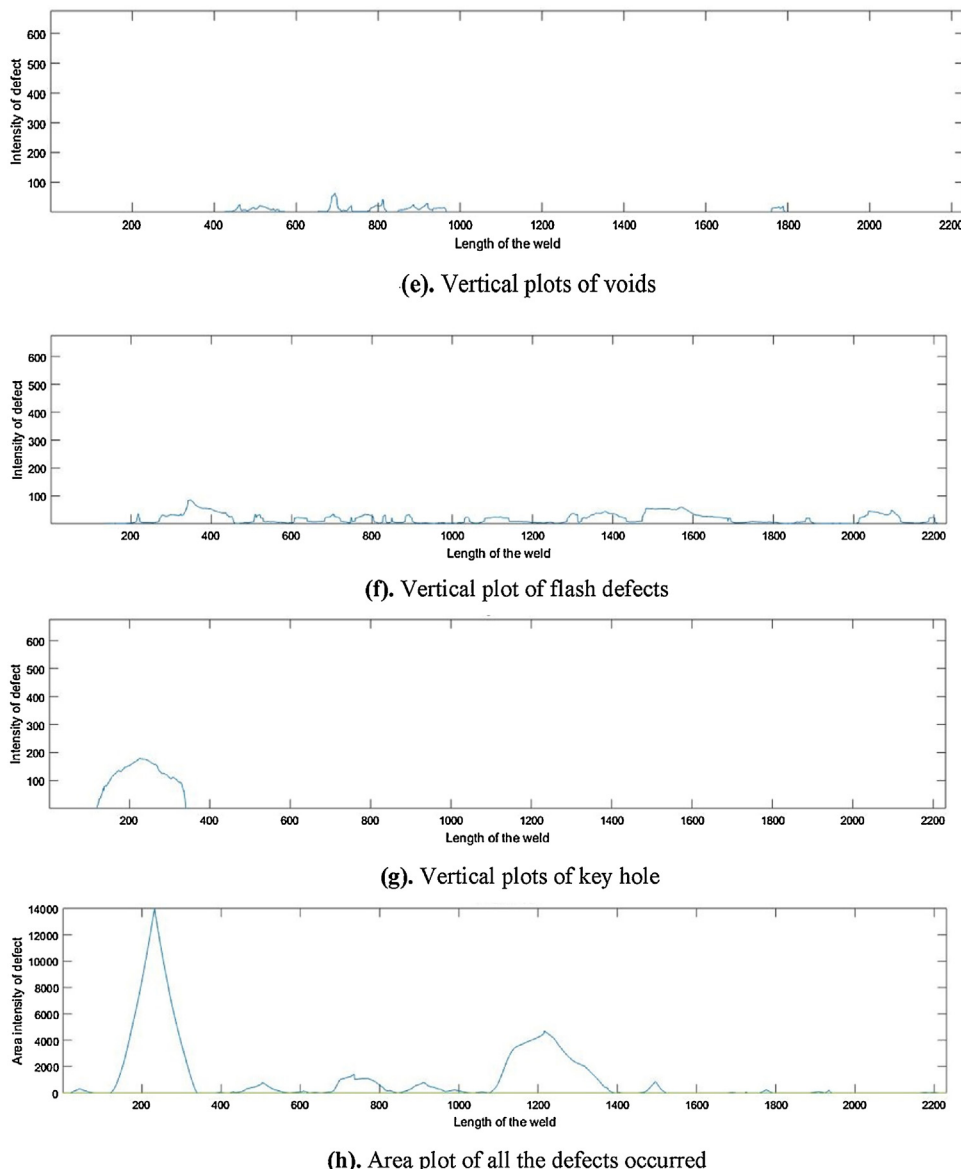


Fig. 12. (Continued).

5. Conclusion

The surface defects in FSW process are identified and have been classified for the first time by using two different image processing techniques. The defects occurred during FSW have been classified into voids, grooves, rough surface texture, flash and key-hole using their unique features. Localization and severity of a surface defect are predicted using the vertical intensity plot corresponding to each type of defect. Additionally, the area plot gives the density of all kinds of defects in a cross-section of the weld bead surface which can be used to analyze the percentage of good weld that occurred. As discussed the proposed research will be useful for online feedback control-based welding parameters monitoring system to improve the weld quality.

Acknowledgment

The authors are grateful to the state of the art facility on friction stir welding in the department of Mechanical Engineering at IIT, Kharagpur.

References

- [1] Thomas WM, Nicholas ED, Needham JC, Murch MG, Templesmith P, Dawes CJ. G.B. Patent 9125978.8, 1991.
- [2] Toros S, Ozturk F, Kacar I. Review of warm forming of aluminum–magnesium alloys. *J Mater Process Technol* 2008;207(1–3):1–12.
- [3] Elangovan K, Balasubramanian V. Influences of pin profile and rotational speed of the tool on the formation of friction stir processing zone in AA2219 aluminium alloy. *Mater Sci Eng A* 2007;459:7–18.
- [4] Nandan R, Debroy T, Bhadeshia HKDH. Recent advances in friction stir welding: process, weldment and properties. *Prog. Mater Sci* 2008;53:980–1023.
- [5] Jain R, Kumari K, Kesharwani RK, Kumar S, Pal SK, Singh SB, et al. Friction stir welding: Scope and recent development. In: Davim J.P., editor. *Modern Manufacturing Engineering*. 2015, p. 179–228.
- [6] Kim YG, Fujii H, Tsumura T, Komazaki T, Nakata K. Three defect types in friction stir welding of aluminum die casting alloy. *Mater Sci Eng A* 2006;415:250–4.
- [7] Chen HB, Yan K, Lin T, Chen SB, Jaing CY, Zhao Y. The investigation of typical welding defects for 5456 aluminium alloy friction stir welds. *Mater Sci Eng A* 2006;433:64–9.
- [8] Joshi V, Balasubramanian K, Prakash RV. Study of defects in friction stir welded AA 5083 by radiography, ultrasonic and phased array ultrasonic technique. Proceedings of the national seminar and exhibition on non-destructive evaluation 2011.
- [9] Saravanan T, Lahiria BB, Arunmuthua K, Bagavathiappan S, Sekhar AS, Pillai VPM, et al. Non-destructive evaluation of friction stir welded joints by X-ray radiography and infrared thermography. *Sci Direct, Procedia Eng* 2014;86:469–75.

- [10] Mężyk J, Kowieski S. The application of thermal imaging method for monitoring the FSW processes. In: Proceedings of the 11th international symposium on measurement and quality control. 2013.
- [11] Lamarre A, Dupuis O, Moles M. Comprehensive inspection of friction stir welds using arrays. In: Proceeding from materials solution on joining of advanced and specialty materials. 2003.
- [12] Cosmi F, Cristofori A, Mancini L, Tovo R, Tromba G, Volpone M. Preliminary investigation by synchrotron radiation of cracks and defects in AA FSW samples. In: Proceedings of the 11th international conference on fracture. 2005 [Research work No. 54–50].
- [13] Wang ZZ. A laser back-lightning based metal transfer monitoring system for robotic gas metal arc welding. *Robot Comput-Integr Manuf* 2016;38:52–66.
- [14] Wang ZZ. Monitoring of GMAW weld pool from the reflected laser lines for real-time control. *IEEE Trans Ind Inform* 2014;10(4) [November].
- [15] Wang ZZ, Zhang Y. Brightness-based selection and edge detection-based enhancement separation algorithm for low-resolution metal transfer images. *IEEE Trans Autom Sci Eng* 2009;6:181–7.
- [16] Wang ZZ, Zhang Y. Image processing algorithm for automated monitoring of metal transfer in double-electrode GMAW. *Meas Sci Technol* 2007;18:2048–58.
- [17] Dhanasekar B, Ramamoorthy BDr. Evaluation of surface roughness using image processing and machine vision system. *J Metrol Soc India* 2006;21:9–15.
- [18] Sinha P, Muthukumaran S, Mukherjee SK. Analysis of first mode of metal transfer in friction stir welded plates by image processing technique. *J Mater Process Technol* 2008;197:17–21.
- [19] Rajashekhar R, Rajaprakash BM. Digital image processing of friction stir weld bead surface using profiling and contouring for weld quality assessment. *IOSR J Mech Civ Eng (IOSR-JMCE)* 2013;5:54–64.
- [20] Rajashekhar R, Rajaprakash BM. Analysis of banded texture of friction stir weld bead surface by image processing technique. *Int J Eng Res Dev* 2013;5:30–9.
- [21] Bhat NN, Kumari K, Dutta S, Pal SK, Pal S. Friction stir weld classification by applying wavelet analysis and support vector machine on weld surface images. *J Manuf Process* 2015;20:274–81.
- [22] Cox CD, Gibson BT, Strauss AM, Cook GE. Energy input during friction stir spot welding. *J Manuf Process* 2014;16:479–84.
- [23] Gibson BT, Lammlein DH, Prater TJ, Longhurst WR, Cox CD, Ballun MC, et al. Friction stir welding: process, automation, and control. *J Manuf Process* 2014;16:56–73.
- [24] Kim D, Kim T, Park YW, Sung K, Kang M, Kim C, et al. Estimation of weld quality in high frequency electric resistance welding with image processing. *Weld J* 2007;71:80 [March].
- [25] Zhang W, Liu Y, Wang X, Zhang YM. Characterization of three-dimensional weld pool surface in GTAW. *Weld J* 2012;91:195–203.
- [26] Meyer F. Topographic distance and watershed lines. *Signal Process* 1994;38:113–25.
- [27] Jain A. Fundamentals of digital image processing. Englewood Cliffs, NJ: Prentice-Hall; 1986. p. 408.
- [28] Adelson EH, Anderson CH, Bergen JR, Burt PJ, Ogden JM. Pyramid methods in image processing. *RCA Eng* 1984;33–41 [November/December].
- [29] Zuiderveld K. Contrast limited adaptive histogram equalization. In: Graphic gems IV. San Diego: Academic Press Professional; 1994. p. 474–85.
- [30] Vincent L. Morphological grayscale reconstruction in image analysis: applications and efficient algorithms. *IEEE Trans Image Process* 1993;2: 176–201.
- [31] MATLAB and image processing toolbox release. Natick, Massachusetts, United States: The Math Works, Inc.; 2012.
- [32] Lim JS. Two-dimensional signal and image processing. Englewood Cliffs, NJ: Prentice Hall; 1990. p. 469–76.
- [33] Burt A. The Laplacian pyramid as a compact image code. *IEEE Trans Commun* 1983;COM-31:532–40.
- [34] Canny J. A computational approach to edge detection. *IEEE Trans Pattern Anal Mach Intell* 1986;PAMI-8:679–98.
- [35] Gonzalez RC, Woods RE, Eddins SL. Digital image processing using MATLAB. USA: Gatesmark Publishing; 2009.